On the Structure and Formation of UTLS PV Dipole/Jetlets in Tropical Cyclones by Convective Momentum Surges

MATTHEW H. HITCHMAN AND SHELLIE M. ROWE

Department of Atmospheric and Oceanic Sciences, University of Wisconsin–Madison, Madison, Wisconsin

(Manuscript received 2 July 2018, in final form 30 July 2019)

ABSTRACT

The structure and origin of mesoscale jets and associated potential vorticity (PV) dipoles in the upper troposphere and lower stratosphere (UTLS) in tropical cyclones (TCs) are investigated. UTLS PV dipole/jetlets, which occurred in Talas (2011), Edouard (2014), and Ita (2014), are simulated with the University of Wisconsin Nonhydrostatic Modeling System (UWNMS). PV dipoles are confined to the UTLS, where the jetlets oppose the ambient anticyclonic flow. They form ~100–250 km from the eye in convective asymmetries and are characterized by surges of air that accelerate in the updraft, overshoot, and extend radially outward. In these cases, the outflow jet merges with the subtropical westerly jet. Analysis of the structure of UTLS PV dipole/jetlets led to a new physical interpretation for their formation, based on the difference in momentum between the updraft and air in the UTLS: the convective momentum transport hypothesis. This view is complementary to the vorticity tilting hypothesis. A jetlet will form whenever an updraft carries horizontal winds to a level with different wind. Schematic diagrams show how to predict jetlet orientation based on horizontal speeds in the updraft and UTLS ambient air. In TCs, horizontal winds in the updraft are cyclonic, so a UTLS jetlet will be cyclonic and oppose the ambient flow. Each jetlet creates an anticyclonic, inertially unstable PV member, which lies radially outward. Estimates of terms in the PV conservation equation support the hypothesis that the dipoles arise from the curl of shear stress. Convective asymmetries associated with PV dipole/jetlets can significantly modify TC evolution by local thermodynamic acceleration.

1. Introduction

This paper describes case studies of tropical cyclones (TCs) where local momentum surges associated with convective asymmetries created pronounced mesoscale jetlets, hence vorticity dipoles, in the upper troposphere/lower stratosphere (UTLS). Analysis of the structure of local wind speed maxima associated with UTLS jetlet/PV dipoles has led to new insight into how they are formed, based on the difference between horizontal momentum within the updraft and air in the UTLS. This led to further consideration of the role of local accelerations in TC convective asymmetries.

Snyder et al. (2007) and Hernandez-Duenas et al. (2014) studied idealized vorticity dipoles in the context of gravity wave radiation during the adjustment process. Davies-Jones (1984), Montgomery et al. (2006) and Chagnon and Gray (2009) showed that PV dipoles can be formed by updrafts in shear, with tilting of horizontal vorticity into the vertical on either side of the updraft. Hitchman and Rowe (2017, hereafter HR17) studied PV dipoles above deep convection in the University of Wisconsin Nonhydrostatic Modeling System (UWNMS) and compared UTLS PV dipoles for the midlatitude "Super Tuesday" cyclone of February 2008 and Tropical Cyclone Talas of September 2011. The contribution to Ertel's potential vorticity $(\zeta + f)/\sigma$, where $\sigma = -(1/g)(\partial p/\partial\theta)$, associated with the vertical component of absolute vorticity is given by $P = (1/\rho)(\partial\theta/\partial z)(\zeta_z + f)$, where $\zeta_z = (\partial v/\partial x) - (\partial u/\partial y)$ is the vertical component of relative vorticity, $f = 2\Omega\sin\phi$ is the vertical component of Earth's vorticity, Ω is Earth's rotation rate, θ is potential temperature, and ρ is density (Andrews et al. 1987). HR17 found PV dipoles of order ±10–100 PVU (1 PVU = 10^{-6} K m^2 kg^{-1} s^{-1}) that were sharply confined to the UTLS. The negative PV members were inertially unstable, consistent with the criterion $f(\zeta_z + f) < 0$. Their analysis confirmed

Supplemental information related to this paper is available at the Journals Online website: https://doi.org/10.1175/MWR-D-18-0232.1.s1.

Corresponding author: Shellie M. Rowe, rowe1@wisc.edu

DOI: 10.1175/MWR-D-18-0232.1

that the tilting term for an updraft in ambient upper-tropospheric shear can account for the PV dipoles.

HR17 suggested the rule of thumb that the negative PV anomaly lies to the left of the ambient wind shear in the upper troposphere, or radially outward in NH TCs. This general relationship is confirmed in UWNMS simulations of 15 TCs. Tilting of horizontal vorticity by an updraft will produce a vorticity dipole. This can happen at any level and is not confined to the UTLS. We have found that jetlets associated with UTLS PV dipoles generally oppose the ambient flow in the UTLS. They tend to be more common east of the eye, where they often extend poleward and merge with the subtropical westerly jet (SWJ). A distinctive feature is that the updraft coincides with horizontal winds that exceed the speed of surrounding air.

The first theme of this paper is to describe the structure of UTLS jetlet/PV dipoles in TCs, including the updraft and outflow jetlet. Analysis of these results provides the basis for a new hypothesis regarding their formation by vertical momentum transport in the updraft, the second theme of this paper. In isentropic analysis, a PV dipole can be generated by the curl of shear stress resulting from a spatially confined wind maximum impinging from below. Consideration of the role of zonally asymmetric momentum surges in TC energetics is the third theme of this work.

Section 2 summarizes recent research on TCs and the role of convective asymmetries. Section 3 describes two closely related mechanisms for PV dipole formation: the updraft tilting of horizontal vorticity hypothesis, then our new convective momentum transport hypothesis. Data and analysis methods are described in section 4. A wide variety of sizes and locations of UTLS PV dipole/jetlets have been found in TC simulations. Three cases were selected for studying the 3D morphology of local wind maxima and UTLS jetlets. Sections 5 and 6 present case studies of TC Talas and Hurricane Edouard from the NH, focusing on the 3D mesoscale structure of the vertically continuous horizontal wind speed maxima and merger with the SWJ. Section 7 presents a case study of Hurricane Ita, an example of jetlet/dipole orientation from the SH. The development of each PV dipole is associated with a momentum surge from the midtroposphere into the UTLS. In section 8 the convective momentum hypothesis of UTLS PV dipole/jetlet formation is discussed further. The mechanism is shown to correspond to a forcing term in the PV conservation equation. Vertical momentum flux convergence associated with the tilted updraft, and vertical advection of horizontal momentum are each shown to be adequate to explain acceleration in the outflow jet. Section 9 includes discussion of the energetics of convective momentum surges and the distribution of radial and tangential winds. Conclusions are given in section 10.

2. Tropical cyclones and convective asymmetries

Theories regarding the formation and intensification of TCs are summarized by Montgomery and Smith (2014), including conditional instability of the second kind (CISK; Charney and Eliassen 1964; Ooyama 1964; Carrier 1971), cooperative intensification (Ooyama 1969; Willoughby 1995), and wind-induced surface heat exchange (WISHE; Emanuel 1986). Wirth and Dunkerton (2006) showed that essential vortex properties of an axisymmetric idealized state are controlled by the rate of thermal relaxation and strength of surface friction.

Axisymmetric models have been widely accepted for their successful description of many features of observed TCs, yet TCs usually exhibit substantial asymmetric structures, which often develop as a partial secondary eyewall (e.g., Didlake et al. 2017, 2018). Several authors have argued that deep convective clusters act to accelerate TC growth (e.g., Heymsfield et al. 2001; Molinari and Vollaro 2010; Guimond et al. 2010; Fang and Zhang 2011; Reasor et al. 2013). The importance of asymmetries in TC convection was explored in idealized numerical studies by Montgomery et al. (2006) and Van Sang et al. (2008). Montgomery and Smith (2014) characterized intensifying TCs as highly asymmetric, with bursts of regional convection coinciding with intensification. Persing et al. (2013), Smith et al. (2014), Wang (2014), and Frisius (2015) found that locally strong eddy processes contribute to strengthening of maximum velocity and extension throughout a TC. Rogers et al. (2016) found that deep convection was preferred in quadrants tied to low-level convergence and high winds. Huang et al. (2018) found that ''nonlinear unbalanced dynamical processes'' contribute significantly toward strengthening, and that upward advection helps to distribute momentum throughout a TC. Fang et al. (2017) showed that during intensification of Edouard the upward mass flux was dominated by asymmetric convection.

The equations of motion in Cartesian coordinates (x, y, z) are

$$\frac{du}{dt} = fv - \frac{1}{\rho}\frac{\partial p}{\partial x} + F_x,$$

$$\frac{dv}{dt} = -fu - \frac{1}{\rho}\frac{\partial p}{\partial y} + F_y,$$

and

$$\frac{dw}{dt} = -g - \frac{1}{\rho}\frac{\partial p}{\partial z} + F_z, \tag{1}$$

where $d/dt = \partial/\partial t + u(\partial/\partial x) + v(\partial/\partial x) + w(\partial/\partial z)$ is the material derivative following the motion, the zonal, meridional, and vertical wind components are $u = dx/dt$, $v = dy/dt$, $w = dz/dt$, and $\mathbf{F} = (F_x, F_y, F_z)$ represents the "viscous force" caused by gradients in stress. The radial symmetry of TCs invites analysis in cylindrical coordinates (r, θ, z), with radial component $u = dr/dt$ ("secondary flow," positive outward), and tangential component $v = rd\theta/dt$ ("primary flow," positive cyclonic in the NH):

$$\begin{aligned}
\frac{du}{dt} - \frac{v^2}{r} - fv &= -\frac{1}{\rho}\frac{\partial p}{\partial r} + F_r,\\
\frac{dv}{dt} + \frac{uv}{r} + fu &= \frac{1}{\rho}\frac{\partial p}{r\partial \theta} + F_\theta,\\
\frac{dw}{dt} &= -g - \frac{1}{\rho}\frac{\partial p}{\partial z} + F_z,
\end{aligned} \tag{2}$$

where $d/dt = \partial/\partial t + u(\partial/\partial r) + v(\partial/r\partial\theta) + w(\partial/\partial z)$ (e.g., Huang et al. 2018). The sum of forces on the rhs causes an acceleration in a fixed coordinate system, which is equal to the sum of accelerations in the rotating coordinate system, plus around the center of the cyclone (curvature terms), and around Earth's rotation axis (Coriolis terms).

Gradient wind balance for the tangential flow in the first equation in (2) occurs when $v^2/r + fv - (1/\rho)(\partial p/\partial r) = 0$. The sum of these three terms is the "gradient balance residual" (Didlake and Houze 2011) or "agradient force" (Abarca et al. 2016). Its departure from zero implies departures from gradient and thermal wind balance and a larger Rossby number, $\mathrm{Ro} = U/(fL)$, where U and L are velocity and length scales. If the inward-directed PGF exceeds the curvature and Coriolis effects, the sum will be negative and the radial flow, u, will accelerate inward [first equation in (2)]. From the second equation in (2), the Coriolis torque on the inward flow will accelerate the tangential flow v. A local azimuthal pressure gradient can also accelerate the tangential flow, hence local angular momentum is not conserved.

Assuming typical TC scales of $U \sim 30\,\mathrm{m\,s^{-1}}$ and $L \sim 300\,\mathrm{km}$, $\mathrm{Ro} \sim 1$. For UTLS jetlets, $U \sim 30\,\mathrm{m\,s^{-1}}$ and $L \sim 100\,\mathrm{km}$, so $\mathrm{Ro} \sim 3$. Acceleration and small-scale processes are important for TCs, increasingly so for mesoscale phenomena. When a low pressure center forms, inward radial flow in the boundary layer creates higher tangential wind speeds via the Coriolis effect. For small Ro, the thermal wind law is expected to be a good approximation of vertical wind shear for the primary circulation: $\partial v/\partial z = (g/fT)(\partial T/\partial r)$. Approximate thermal wind balance has been diagnosed in axisymmetric models of TCs and mature TCs. A warm core TC constrains the shear to be anticyclonic above the maximum cyclonic flow from the top of the boundary layer to the UTLS. However, where strong vertical motions and local accelerations occur, Ro is expected to be large, and the distribution of tangential winds may depart significantly from thermal wind balance. In the case studies shown below, the distribution of tangential winds is similar to balanced vortex theory in some regions but exhibits significant departures near convective asymmetries.

Holland and Merrill (1984) suggested that an outflow jet interacting with a trough could strengthen convection and enhance deepening, and that weak inertial instability played an important role. Wu and Cheng (1999) studied the evolution of PV and wind in typhoon outflow layers. Bosart et al. (2000) found a significant increase in upper-tropospheric divergence poleward of Opal just prior to intensification. Rappin et al. (2011) found that idealized TCs often display two large outflow regions, linked to areas of weak inertial stability. Komaromi and Doyle (2017) showed that, in 6 TCs sampled by dropsonde, outflow originates in a region of low inertial stability in the layer 300–150 hPa at 50–200 km radius. In this study, the origin of low inertial instability in UTLS outflow is described in terms of the aggregation of negative members of PV dipole/jetlets formed by local deep convection.

3. UTLS PV dipole formation

In this paper, we attempt to unify three perspectives of the same dipole formation process: vortex tilting (traditional), convective momentum transport (intuitive), and isolated stress (PV budget equation). A more complete discussion of the latter will be given in section 8, after presenting the case studies.

a. Vorticity tilting hypothesis of PV dipole/jetlet formation

Davies-Jones (1984, Fig. 7) illustrated how an updraft can create a pair of counter-rotating horizontal vortices by tilting of horizontal shear. This process was also described by Montgomery et al. (2006). Chagnon and Gray (2009) used the linearized Boussinesq equations to show that horizontal PV dipoles can be created by tilting horizontal vorticity into the vertical. They emphasized that the ambient vorticity associated with vertical shear is produced by latent heating at the cyclone scale, a prerequisite for updraft tilting of vorticity. Markowski and Richardson (2010) explored the role of vertical motion in bending horizontal vorticity into a horseshoe shape during tornadogenesis.

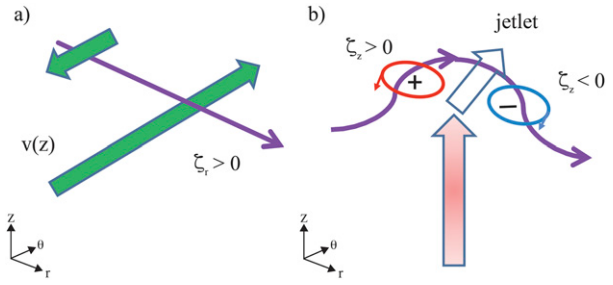

FIG. 1. A schematic diagram of PV dipole formation based on the vorticity-tilting hypothesis of Montgomery et al. (2006) and Chagnon and Gray (2009), applied to a TC in the NH, whereby tilting of horizontal vorticity by an updraft can produce a dipole of vertically oriented vorticity. Consider a convective cluster a few hundred km radially outward from the eye, where (a) cyclonic flow in the midtroposphere (tangential velocity v, green arrows) becomes anticyclonic in the UTLS, such that horizontal vorticity (purple arrow) is directed radially outward in the upper troposphere ($\zeta_r > 0$), and (b) a convective updraft (pink arrow) will bend horizontally oriented vorticity into a horseshoe shape, creating a horizontal dipole in vertical vorticity (ζ_z). A dipole in vorticity will have a jetlet in between, which, in this situation, opposes the ambient anticyclonic circulation in the UTLS. The negative vorticity center (blue) lies to the left of the upper-tropospheric (anticyclonic) shear and lies radially outward.

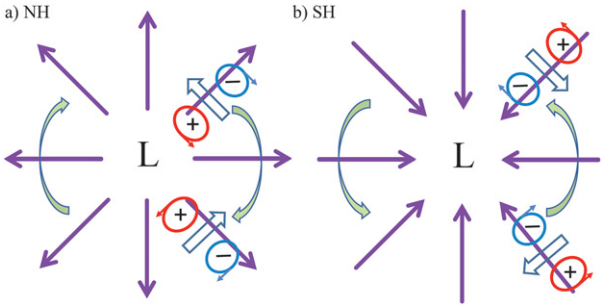

FIG. 2. Prediction of PV dipole/jetlet orientation in a TC, based on the updraft tilting hypothesis (Fig. 1) for the (a) NH and (b) SH. The location of the TC center is indicated with an "L." Green arrows indicate the ambient anticyclonic upper-tropospheric shear, while purple arrows indicate the associated horizontal vorticity, which is directed radially outward in the NH, and inward in the SH. The resulting jetlets oppose the UTLS anticyclonic circulation. The tilting hypothesis predicts that the unstable member lies radially outward. Each dipole can contribute to the aggregated outflow of low PV air in the UTLS.

HR17 studied UTLS PV dipoles above deep convection in midlatitude cyclones (MCs) and TCs and concluded that they could be explained by the vortex tilting hypothesis. They suggested two rules of thumb: 1) A convective updraft will generate a negative PV anomaly to the left of the ambient wind shear direction. 2) The anomalous (inertially unstable) member will lie radially outward in a TC.

In Cartesian coordinates, the tilting term in the conservation equation for absolute vorticity can generate horizontal dipoles according to

$$\frac{D}{Dt}(\zeta_z + f) = -\left(\frac{\partial w}{\partial x}\frac{\partial v}{\partial z} - \frac{\partial w}{\partial y}\frac{\partial u}{\partial z}\right) \tag{3}$$

or

$$\frac{D}{Dt}(\zeta_z + f) = -\left(\frac{\partial w}{\partial r}\frac{\partial v}{\partial z} - \frac{\partial w}{r\partial\theta}\frac{\partial u}{\partial z}\right) \tag{3′}$$

in cylindrical coordinates, where $\zeta_z = (1/r)[\partial(rv)/\partial r] - (\partial u/r\partial\theta)$ [cf. (2)]. In a NH TC, $\partial v/\partial z < 0$ in the upper troposphere, so that a buoyant updraft will tilt horizontal vorticity downward on the radially outward side and upward on the inward side.

Figure 1 presents a schematic view of the process by which an updraft penetrating a preexisting vorticity sheet can create a PV dipole. It is based on the same principle as that shown in Fig. 10 of Montgomery et al. (2006), but applied to the geometry of a TC. In the NH, cyclonic azimuthal flow is strong in the troposphere, diminishing upward and reversing to anticyclonic flow in the UTLS (green arrows in Fig. 1a). The anticyclonic shear in the upper troposphere is associated with horizontal vorticity, which is directed radially outward ($\zeta_r > 0$, purple arrow in Fig. 1a). An updraft can bend the horizontal vorticity into a horseshoe shape, with horizontal vorticity tilted upward on the inward side ($\zeta_z > 0$) and downward on the outward side ($\zeta_z < 0$) (Fig. 1b). The negative vorticity anomaly lies radially outward. The jetlet between the dipole is directed cyclonically, which is in the opposite direction to the large-scale anticyclonic outflow in the UTLS.

The relationship between anticyclonic upper-tropospheric wind shear, horizontal vorticity, and the expected orientation of vorticity dipole/jetlets is shown for the NH and SH in Figs. 2a and 2b. The anticyclonic member lies to the left of the upper-tropospheric anticyclonic shear and lies radially outward in both hemispheres.

b. *Convective momentum transport hypothesis of jetlet/PV dipole formation*

A convective momentum transport hypothesis is proposed for the origin of a UTLS jetlet/PV dipole. In this view, an updraft impinging on the stratosphere will exert a spatially limited force, thereby inducing two counter-rotating vortices, similar to a canoe paddle drawn through water. This "source term" in the PV conservation equation is assessed in section 8. The marked upward increase in static stability at the tropopause effectively limits the updraft penetration and concentrates the momentum outflow in the UTLS.

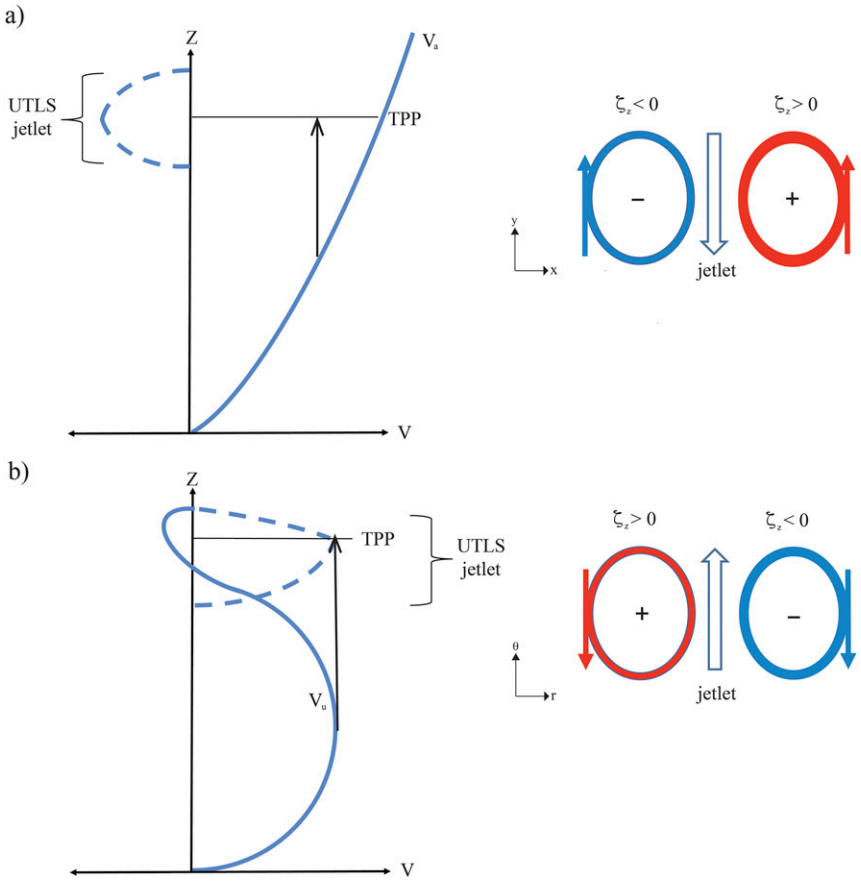

FIG. 3. Schematic diagram of the vertical momentum transport hypothesis for UTLS jetlet/PV dipole formation in the case where (a) horizontal speed in the updraft is less than in the UTLS, creating a jetlet *that opposes the midtropospheric flow*, and (b) horizontal cyclonic momentum in the updraft exceeds that in the UTLS, creating a jetlet *that is in the same direction as the midtropospheric flow*. Case (b) is most relevant for convective momentum surges in TCs.

This convective momentum transport hypothesis is applicable to any situation of deep convection. Consider the following two situations: 1) air in the updraft is moving more slowly than the ambient air, v_a, in the UTLS; 2) air in the updraft, v_u, is moving faster than in the UTLS; and the two special cases of 3) no vertical shear, and 4) a symmetric ring of convective updrafts. In case 3, since there is no speed difference, this theory predicts that there would be no jetlets or dipoles. In case 4, such as an axisymmetric inner eyewall, this theory predicts no jetlets or dipoles, because individual jetlets would blend into a symmetric tangential flow, as in a symmetric inner eyewall. Instead of dipoles, an inner ring of high PV air would form on the inner flank of the tangential flow maximum, with a ring of low PV air on its outer flank.

Cases 1 and 2 are shown in Fig. 3. A "stratospheric cap" is imposed on the profiles such that $v_u(z) \rightarrow 0$ above the tropopause. In Case 1) (Fig. 3a), where horizontal speed in the updraft is less than ambient air, upward transport will cause a jetlet directed opposite to the flow, such that the anticyclonic member lies to the left of the wind shear and to the left of the prevailing wind direction. This case includes Malkus' (1952) work, where the horizontal speed in the updraft was assumed to be fixed at the lifting condensation level, and is therefore less than the ambient speed in linear shear. This is the situation in Fig. 7 of Davies-Jones (1984). This case is also relevant for convection occurring in the poleward flow to the east of a trough in a MC, where the poleward shear extends well into the stratosphere (Rowe and Hitchman 2016).

Case 2 (Fig. 3b) is most relevant for TCs, where cyclonic flow in the midtroposphere is transported into the anticyclonic ambient flow of UTLS, yielding a striking difference in speed (dashed profile). This speed difference is more pronounced when winds accelerate during ascent. Since the jetlet is directed

cyclonically, the negative PV anomaly must lie to the right of the jetlet (Fig. 3b).

The predicted orientation of UTLS PV dipole/jetlets in TCs based on the vertical momentum transport hypothesis is shown in Fig. 4 for the NH and SH. Cyclonic midtropospheric flow (green arrows) injected into the UTLS causes cyclonically oriented jetlets, with negative PV to the right of midtropospheric flow, and anomalous PV lying radially outward.

The complementarity between the two hypotheses may be seen mathematically as follows. As the updraft arrives in the UTLS, the flow will accelerate due to vertical advection: $\partial v/\partial t \sim -w(\partial v/\partial z)$. Taking $\partial/\partial x$ of this relation generates $(\partial/\partial t)(\partial v/\partial x) \sim (\partial\zeta/\partial t) \sim -(\partial w/\partial x)(\partial v/\partial z)$. Thus, vertical advection of the tangential wind by the updraft in the second equation in (2) corresponds to a tilting term in the vorticity equation (3). This unifies the perspectives shown in Figs. 1 and 3, where updraft tilting of horizontal vorticity and upward transport of horizontal momentum are two ways of looking at the same phenomenon.

4. Data and analysis methods

TCs exhibit considerable diversity in the number, size, and distribution of UTLS PV dipoles. Dipoles and outflow jets tend to increase in area with time, with some exhibiting two large outflow quadrants spanning the entire TC. PV dipoles/jetlets selected for study occurred in TC Talas (2011), Hurricane Edouard (2014), and Hurricane Ita (2014). PV dipoles can occur in any quadrant of a TC. The cases shown here were selected as representative of those that commonly form to the east of the eye. In each case, the TC was undergoing subtropical transition and the jetlet merged with the adjacent SWJ.

Studies of processes in the UTLS using the UWNMS include Pokrandt et al. (1996), Hitchman et al. (1999, 2003, 2004), Kittaka et al. (2004), Rowe and Hitchman (2015, 2016), and HR17. The UWNMS was initialized with 2.5° ECMWF data, which then generated mesoscale convection according to model physics. The horizontal resolution of the model for TC Talas (2014) and Hurricane Edouard (2014) was 15 km, and 20 km for Hurricane Ita (2014), with no inner grid nesting. The vertical resolution was 300 m and the model top was set to 28 km for Talas and Edouard and 25 km for Ita. Each simulation was carried out for 48 h, with the convective features of interest forming ~12–24 h into the simulation. Vis5d was used to view the evolving 3D structure of winds and other variables. Isosurfaces of wind speed were

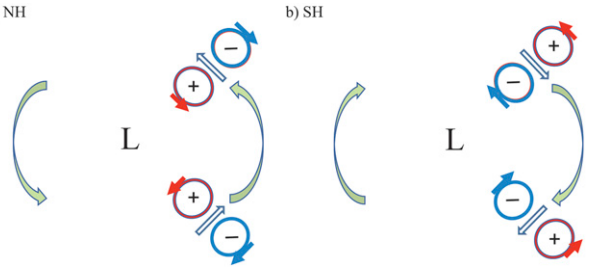

FIG. 4. Prediction of PV dipole/jetlet orientation, based on the vertical momentum transport hypothesis for a TC in the (a) NH and (b) SH. The location of the TC center is indicated with an "L." Here green arrows indicate midtropospheric cyclonic flow. A convective momentum surge will inject midtropospheric flow into the UTLS, causing cyclonically oriented jetlets. This causes a PV dipole, with the anomalous member for that hemisphere appearing to the right of midtropospheric flow, lying radially outward.

calculated using all three components, although $|w| < 5\,\mathrm{m\,s^{-1}}$.

HR17 compared UTLS PV dipole representation at 10, 15, and 20 km resolution. With finer resolution, PV dipole maxima increase in magnitude and contract in size, but the areal extent of individual PV anomalies is similar. In modeling TC Fay, Wang (2014) found that with finer resolution the size of updrafts decrease and number of updrafts increase, but their areal fraction, mean vertical velocity and mass flux were insensitive to resolution.

ECMWF analyses with 0.14° × 0.14° resolution provide a complementary depiction of PV dipoles. Satellite images obtained from the Space Science and Engineering Center (SSEC) were also used to compare the time and location of deep convective clusters. Independent estimates of minimum sea level pressure (SLP) were obtained from the Cooperative Institute for Meteorological Satellite Studies (CIMSS 2018). The UWNMS minimum SLP of ~976 hPa for Talas agreed well with CIMSS estimates. The minimum SLP values for Edouard and Ita were not as low as the CIMSS average, but the spread in CIMSS estimates was much larger than for Talas.

5. Tropical Cyclone Talas (2011)

In late August 2011, TC Talas moved northward over the Philippine Sea, making landfall in Japan on 2 September 2011, bringing ~1.5–2 m of rain in 72 h to the Kii Peninsula (Oku et al. 2014; Japan Meteorological Agency 2011). Figure 5a shows an infrared satellite image of Talas at 1332 UTC 2 September 2011, with center located near 32.5°N, 134°E. Figure 5b shows 100 hPa PV from the 0.14° × 0.14° ECMWF analyses

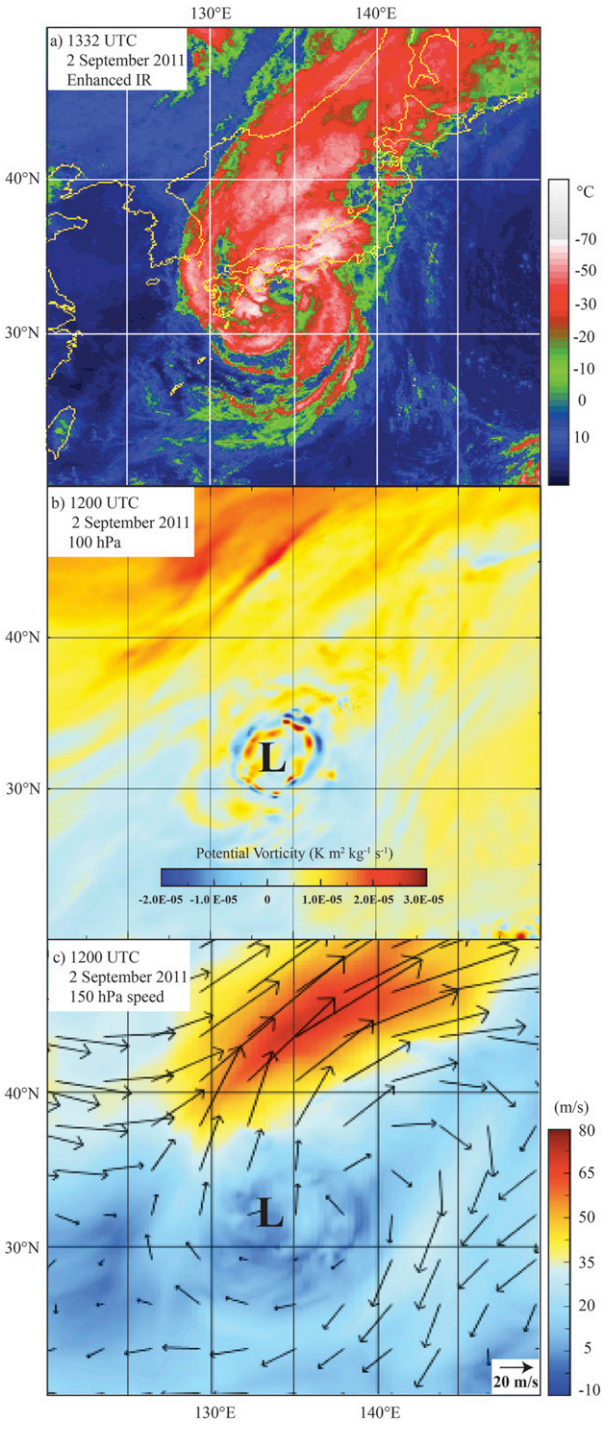

FIG. 5. (a) Enhanced infrared satellite image of Talas at 1332 UTC 2 Sep 2011 (courtesy of SSEC, UW–Madison). ECMWF 0.14° resolution fields at 1200 UTC 2 Sep 2011 of (b) 100 hPa PV (color bar), and (c) 150 hPa wind (color bar, reference vector 20 m s^{-1}). The location of the surface low is indicated by an "L."

at 1200 UTC 2 September 2011, ~1.5 h earlier than the infrared image. A ring of PV dipoles is seen around the eye at a radius of ~200 km, each with the negative member located radially outward, with a strong cluster occurring to the northeast of the eye (Fig. 5b). Figure 5c shows ECMWF 150 hPa winds, with anticyclonic outflow joining with the SWJ on Talas' poleward flank.

The evolution of PV dipoles in TC Talas is shown in Fig. S1 in the online supplemental material, for the 36-h period 0000 UTC 2 September–1200 UTC 3 September. A series of PV dipoles formed ~150–200 km to the east of the eye, which strengthened and propagated northward. The dipole selected for study is located to the north of the eye at 1040 UTC. (The dipole to the northeast of the low during 1600–2000 UTC in Fig. S1 was described in HR17.) In the extratropical transition of Talas, ambient large-scale anticyclonic circulation in the UTLS organized the complex array of PV dipoles into a pair of positive and negative PV streamers on the equatorward side of the SWJ (HR17).

Figure 6 shows the spatial relationship between the updraft, particle trajectories, maximum winds, UTLS PV dipole, and outflow jetlet in the UWNMS simulation of Talas at 1040 UTC 2 September 2011. A view from the southwest is seen in Fig. 6a. The 34 m s^{-1} isosurface indicates a vertically continuous wind speed maximum coincident with a poleward-tilted updraft, which overshoots, subsides, and then continues poleward to join with the SWJ. The speed is less than 34 m s^{-1} everywhere outside of the blue isosurface. The link between the updraft and PV dipole formation is highlighted by 4-h trajectories ending between the UTLS PV dipole at 1040 UTC. They also illustrate the horizontal tilt of air motions typical in a TC. The zenith angle of the trajectories is given by $\tan\alpha \sim (\delta y/\delta z) \sim (250\,\text{km}/17\,\text{km})$, so that $\alpha \sim 86°$ (4° elevation angle). This predominantly horizontal trajectory is compatible with $v \sim 30\,\text{m s}^{-1}$ and $w \sim 3\,\text{m s}^{-1}$, or $|v/w| \sim 10$.

Figures 6b and 6c show meridional sections through the poleward surge shown in Fig. 6a. Air with poleward motion maximizing in the midtroposphere (Fig. 6b) abruptly ascends in the updraft near 35°N, reaches ~17 km altitude, subsides ~2 km as it detrains poleward to ~40°N and merges with the SWJ in an outflow layer ~5 km thick. A PV dipole of ~ −7 and +21 PVU is found confined to the layer ~14–18 km, immediately atop the updraft (Fig. 6c). The inertially unstable member is located in the outflow jet.

Note the PV maximum near 7 km in the updraft, which diminishes to zero by ~13 km. This feature conforms with the mechanism of vortex stretching below and vortex compression above the level of heating maximum (cf. Chagnon and Gray 2009). The updraft in

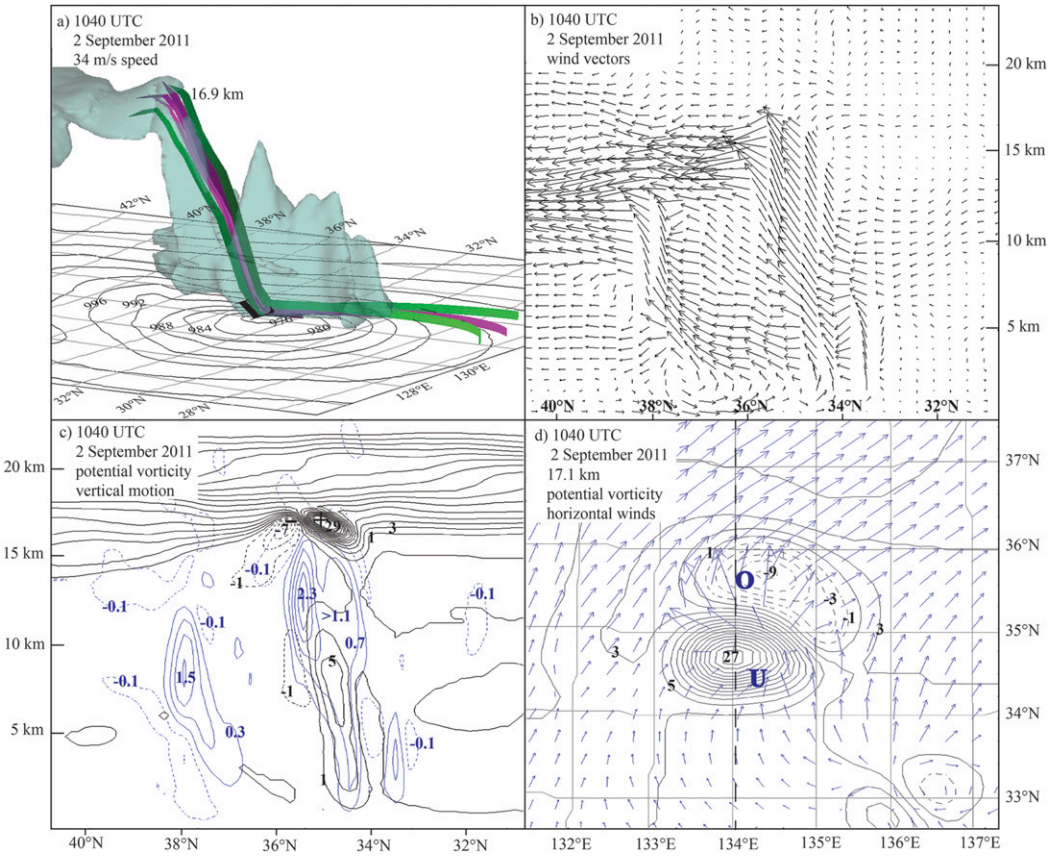

FIG. 6. UWNMS simulation of Tropical Cyclone Talas at 1040 UTC 2 Sep 2011. (a) View from the southwest of SLP contours (interval 4 hPa), a 34 m s^{-1} speed isosurface (blue), and 4-h back trajectories (purple and green ribbons) from the PV dipole. Meridional sections of (b) wind vectors in the plane, and (c) PV (black contours, every 2 PVU) and vertical wind (blue contours, every 1 m s^{-1}). (d) PV (black contours, every 2 PVU) and horizontal winds (arrows, max vector 40 m s^{-1}) at 17.1 km. The locations of soundings in the updraft ("U") and outflow jet ("O") are indicated in (d).

Fig. 6c peaks at ~2 m s^{-1}. At this time, the PV dipole was positioned ~250 km north-northeast of the surface low (Fig. 6d). Air from this jetlet flows northward, then joins the SWJ (cf. Fig. 5c).

Profiles of u, v, and w at the locations of the updraft and outflow jet are shown in Fig. 7. In this case, the updraft terminates in the positive PV anomaly of ~30 PVU (Fig. 6c), with the tropopause located near 16 km. Vertical motion in the updraft exhibits a broad maximum of ~3 m s^{-1} near 10 km in Talas (Fig. 7a), but is less than 0.2 m s^{-1} in the outflow jet profile (Fig. 7b). In general, an updraft will be tilted, so that a vertical sounding will not coincide exactly with the updraft axis. Convective updraft maxima in the UWNMS of 1–5 m s^{-1} are in general agreement with observational estimates of 1–10 m s^{-1} (Austin and Houze 1973), although Houze et al. (2009) documented an updraft of ~10–25 m s^{-1} in a radar study of TC Ophelia.

The meridional wind profile in the updraft exhibits a broad poleward maximum of 25–30 m s^{-1} in the 4–12 km layer (Fig. 7a). The shapes of the v and w profiles are similar in the troposphere, such that the ratio w/v is approximately constant in the updraft (Fig. 6). 150 km downstream there is weak vertical motion and weak meridional flow in the lower and middle troposphere. A strong poleward outflow jet occurs in the layer 12–17 km, with a maximum of 45 m s^{-1} near 16 km (Fig. 7b). Horizontal momentum in the midtroposphere has been concentrated and strengthened into an outflow jet in the UTLS.

The PV dipole shown in Fig. 6 occurred in conjunction with a momentum surge that began in the lower troposphere, accelerated in the updraft, impinged on the base of the stratosphere and continued poleward in the UTLS. Figure 8 shows a sequence of meridional wind profiles following the location of the maximum in horizontal wind speed for the 2-h period 0900–1100 UTC 2 September 2011. The first profile exhibits a speed maximum near 9 km, with subsequent profiles showing the momentum surge being transported in the updraft to

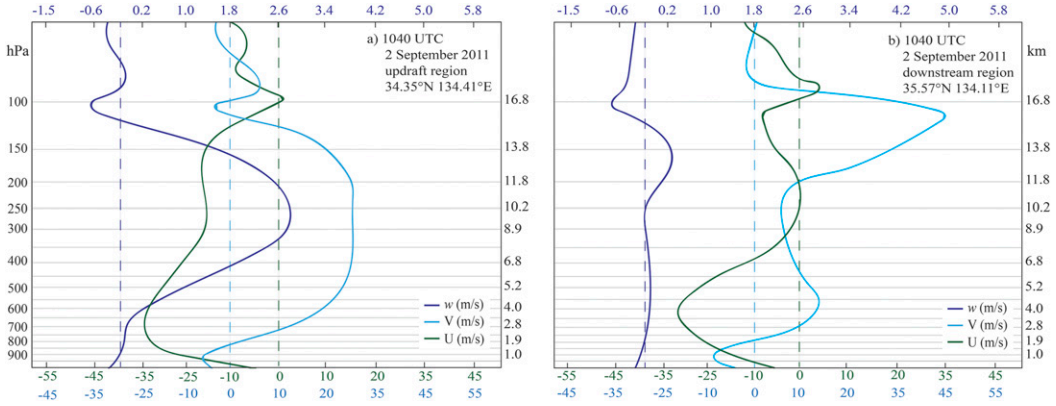

FIG. 7. Profiles of UWNMS wind components (a) in the updraft (location "U" in Fig. 6d) and (b) in the outflow jet ~150 km downstream (location "O" in Fig. 6d) for the Talas PV dipole/jetlet shown at 1040 UTC 2 Sep 2011. Zonal wind (green), meridional wind (light blue), and vertical wind (purple) profiles are indicated with separate scales in m s^{-1}, with vertical dashed lines indicating the zero coordinate for each variable.

~17 km, and then subsiding to ~16 km. The maximum speed increased from 35 to 48, or ~1 m s^{-1} per 10 min.

The horizontal wind speed in the updraft associated with a UTLS PV dipole/jetlet noticeably exceeds that in the surrounding air. This suggests that each convective cluster is converting available energy to kinetic energy more rapidly than in the surrounding air. Since the updraft air is moving faster, drag and mixing will cause the ambient air to accelerate. Similarly, the outflow jet will accelerate the ambient air.

6. Hurricane Edouard (2014)

Figure 9a shows the track of Edouard from its development into a TC on 12 September 2014, intensification into a category 3 hurricane on 16 September to the east of Bermuda, then weakening during 17–18 September as it curved northeastward. Figure 9b shows an enhanced IR image at 0000 UTC 17 September, featuring an eyewall and spiral bands of convection, with significant outflow into the midlatitudes. A convective cluster was located ~200 km to the northeast of the eye, in the "decaying double-eyewall phase" of Edouard (Abarca et al. 2016). The location of the surface low in Fig. 9c near 32.5°N, 57°W was obtained from the ECMWF 1000 hPa relative vorticity chart, and is in good agreement with the IR satellite image. Note the anticyclonic outflow from Edouard, merging with the SWJ near 45°N, 55°W, with speeds exceeding 50 m s^{-1} (Fig. 9c).

In the UWNMS simulation of Edouard, updraft cores were found ~200 km to the northeast of the surface low at 2300 UTC 16 September 2014 (Fig. 10), arranged in a band oriented northwest-southeast (cf. Fig. 9b). Trajectories show the continuous air motion from the boundary layer into the updraft, ejection in the outflow jet, and merger with the SWJ (Fig. 10a). In the

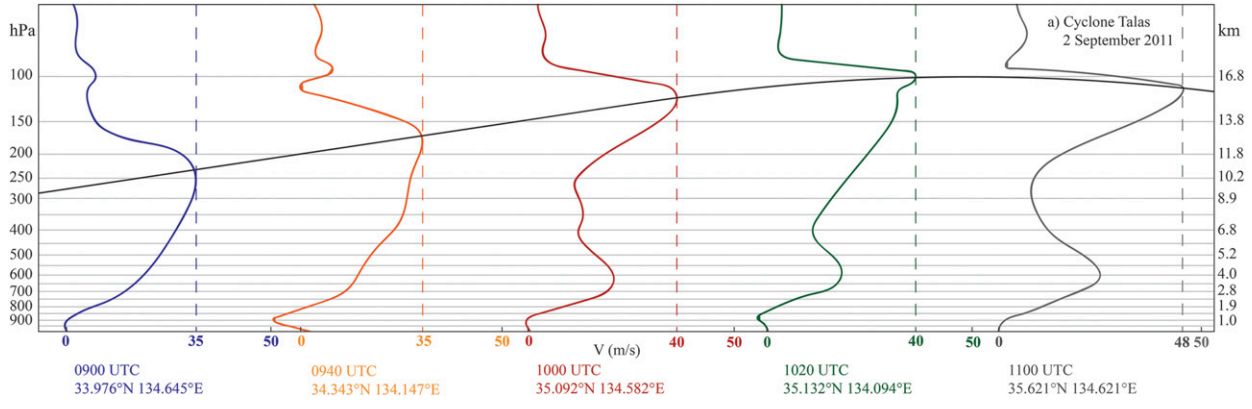

FIG. 8. Time sequence of meridional wind profiles following the momentum surge, which created the UTLS PV dipole/jetlet in Talas shown in Figs. 6 and 7. The locations of wind maxima are connected with a black curve to track the ascent of the surge in the updraft and subsidence in the outflow jet.

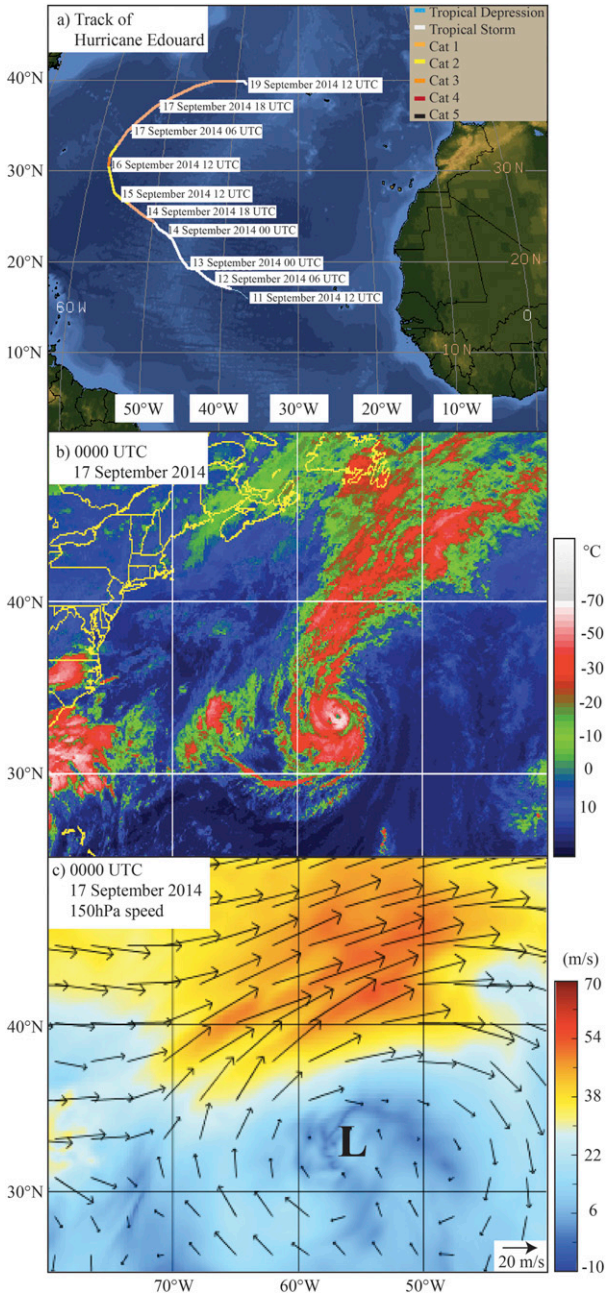

FIG. 9. (a) Track of Hurricane Edouard during 11–19 Sep 2014. (b) Enhanced infrared satellite image at 0000 UTC 17 Sep 2014, courtesy of SSEC, UW–Madison. (c) ECMWF 150 hPa winds at 0000 UTC 17 Sep 2014 (color bar, reference vector length 20 m s^{-1}).

updraft particles ascend $\delta z \sim 14$ km as they travel northward $\delta y \sim 150$ km, such that $\alpha \sim 85°$.

Winds in a meridional section through the updraft are shown in Fig. 10b. South of the updraft, poleward motion maximizes in the lower to midtroposphere, with abrupt ascent in the updraft, followed by poleward detrainment in the outflow jet. The outflow layer is ~5 km thick and descends from ~15 to 13 km altitude across 35°–40°N.

The UTLS PV anomalies are confined to the 13–17 km layer (Fig. 10c). A maximum updraft of ~4 m s^{-1} is evident near 6 km (Fig. 10c). The vertical motion pattern in the stratosphere is consistent with upward and poleward propagation of gravity wave energy away from the UTLS PV dipole, with vertical wavelengths ~7 km and meridional wavelengths ~250 km.

A horizontal view of PV and 3D wind speed at 15.6 km is shown in Fig. 10d. A PV dipole of ~ −4 and +10 PVU is found near 34.5°N, 55.7°W, ~250 km to the northeast of the eye. Poleward flow in the mesoscale wind speed maximum between the PV dipole blends into the SWJ (Fig. 10d).

The updraft terminates in the positive PV anomaly of ~10 PVU, with a tropopause near 15 km (Figs. 10c,d). The vertical motion profile in the updraft exhibits a broad maximum of ~5 m s^{-1} near 7 km (Fig. 11a). Weak vertical motions prevail at all altitudes 150 km downstream (Fig. 11b). The meridional wind profile in the updraft exhibits a poleward maximum of ~30 m s^{-1} near 7 km (Fig. 11a). The shapes of the v and w profiles are similar, such that w/v is approximately constant in the updraft (Fig. 10a). The meridional wind profile near the outflow jet exhibits weak flow in the middle and lower troposphere and strong poleward flow in the layer 10–15 km, with a maximum of 40 m s^{-1} near 14 km (Fig. 11b).

Figure 12 shows a sequence of meridional wind profiles following the location of the maximum in wind speed for the period 1700–2040 UTC 16 September 2014. The first profile exhibits a speed maximum near 7 km altitude, with subsequent profiles showing the momentum surge being transported in the updraft to ~14.5 km altitude, and then subsiding to ~14 km, while the maximum speed increases from 30 to ~62, or ~1 m s^{-1} per 6 min.

Figure S2 shows the evolution of wind speed, vertical motion, and trajectories, as seen from the west. Momentum surges propagate through this convective system, with vertical motions and horizontal wind speed first increasing in the lower troposphere, then middle, then upper troposphere, followed by a poleward surge downstream in the UTLS. These examples support the idea that PV dipoles forms atop deep convection due to a momentum surge in the updraft.

7. Hurricane Ita (2014)

Figure 13a shows the track of Hurricane Ita from its beginnings as a tropical storm near the Solomon Islands on 4 April 2014, development into a category 4 hurricane before making landfall in Queensland on 11 April,

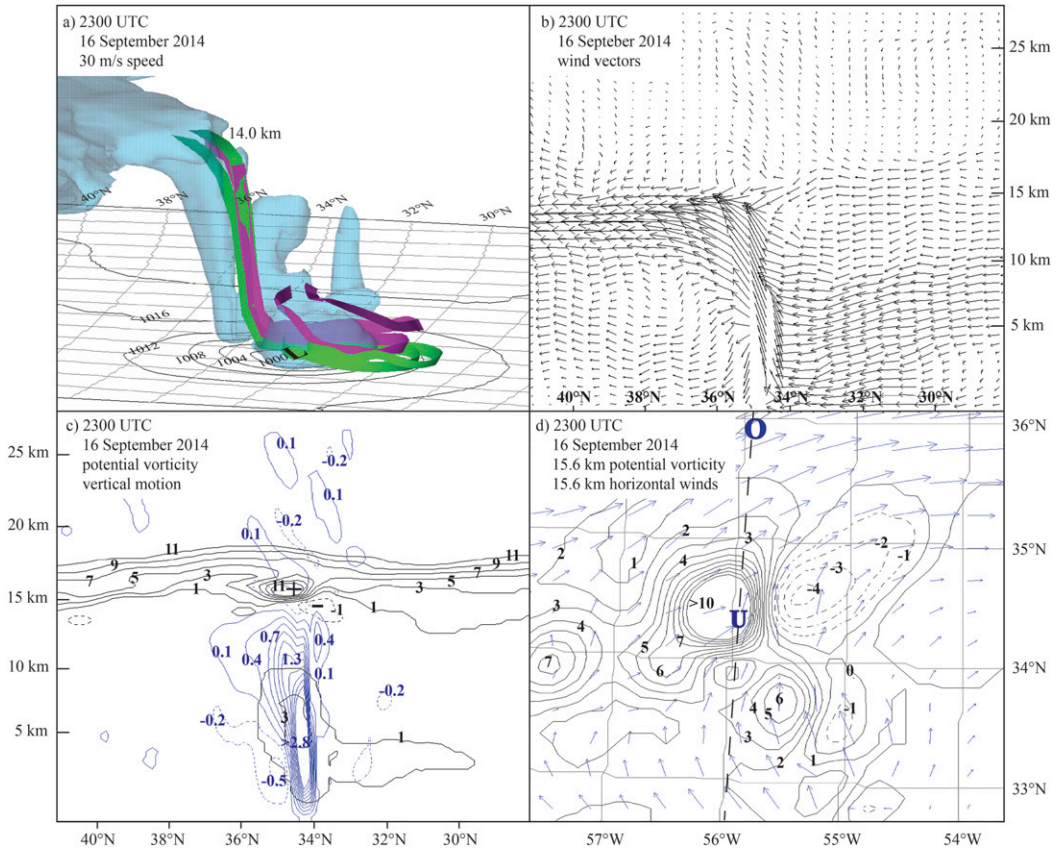

FIG. 10. As in Fig. 6, but for Hurricane Edouard at 2300 UTC 16 Sep 2014, in (b) a speed isosurface of 30 m s^{-1} is shown, and in (d) the level is 15.6 km.

and dissipating over the South Coral Sea on 14 April. A satellite infrared image at 1332 UTC 10 April 2014 (Fig. 13b) shows the eye to be located near 13°S, 146°E, with spiral cloud bands extending toward the equator and as far as 20°S. A convective cluster is located ~300 km to the southeast of the eye, the location of the UTLS PV dipole shown below. Anticyclonic outflow is evident, with poleward flow blending counterclockwise into the SWJ, which exceeds 25 m s^{-1} south of 25°S. In the SH, cyclonic flow in the midtroposphere is clockwise (cf. Fig. 4b), with upper-tropospheric shear directed counterclockwise (Fig. 2b).

The evolution of 16 km PV and winds in the UWNMS on 10 April 2014 is shown in Fig. S3. At 0940 UTC, a PV

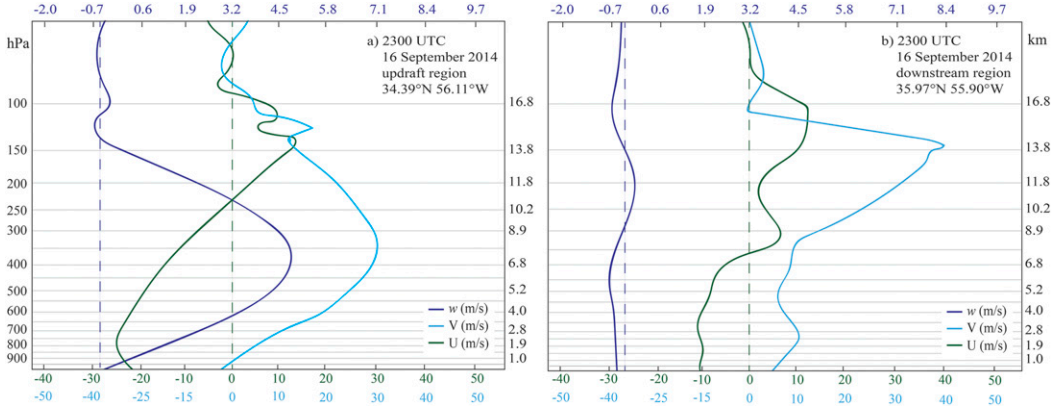

FIG. 11. As in Fig. 7, but for the Edouard PV dipole/jetlet shown in Fig. 10, at 2300 UTC 16 Sep 2014.

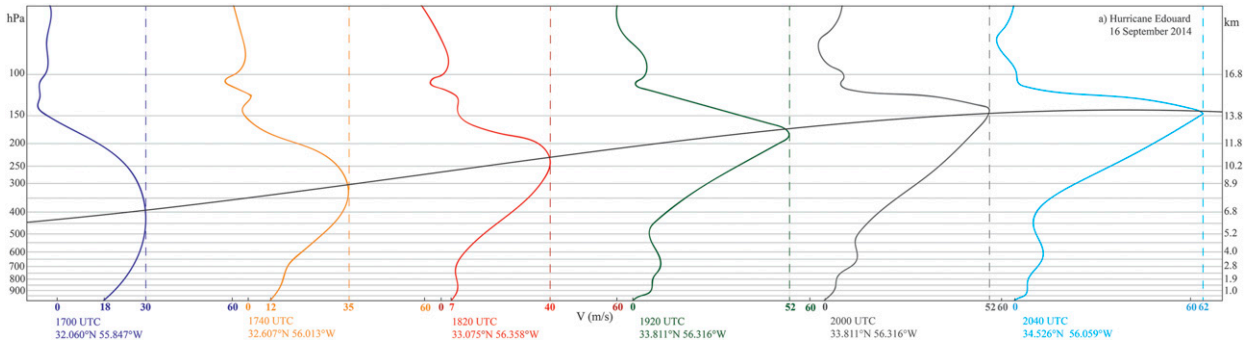

FIG. 12. As in Fig. 8, but for the Edouard PV dipole/jetlet shown in Fig. 10, for the period 1700–2040 UTC 16 Sep 2014.

dipole is found ~100 km to the west of the surface low, with another ~200 km east-southeast of the surface low. The positive (inertially unstable) member of each PV dipole lies radially outward. The low PV anomaly lies to the left of the wind shear. A northwestward jetlet lies between the western PV dipole. These jetlets oppose the anticyclonic UTLS flow, in agreement with Figs. 2b and 4b. The eastern dipole became the dominant location of asymmetric convection, lasting for more than 24 h.

Figure 14 shows the structure of the eastern dipole/jetlet. A view from the northeast of the 30 m s^{-1} speed isosurface and 2-h back trajectories from the PV dipole at 1420 UTC (Fig. 14a) shows the coincidence of the updraft and horizontal speed maximum, the poleward outflow jet, and merging with the SWJ. In a meridional section centered on the updraft (Fig. 14b), midtropospheric cyclonic flow is diverted upward in the updraft and ejected in the outflow jet into the UTLS. The updraft penetrates to ~17 km, above the maximum level of outflow near 15 km (Fig. 14b). At an ascent rate of ~5 m s^{-1}, it takes ~1 h to reach the tropopause. Descent of the outflow layer of ~2 km is observed. This behavior is reflected in the shape of the speed isosurface in Fig. 14a. Again, air in the updraft and outflow jet has anomalously high horizontal wind speeds compared with the surrounding air.

The PV dipole straddles the top of the updraft (Fig. 14c), with a southward outflow jet reaching ~35 m s^{-1} at 16 km (Fig. 14d). Again, the jetlet is oriented in the direction of the midtropospheric flow, confirming Fig. 3b, and the inertially unstable member lies radially outward (as in Fig. 4b).

Soundings in the updraft and ~150 km downstream in the outflow jet (U and O in Fig. 14d) are shown in Fig. 15, with the tropopause located near 16.5 km (Fig. 14c). The vertical motion profile in the updraft exhibits a broad maximum of ~5 m s^{-1} near 9 km (Fig. 15a), but $|w| < 0.5$ m s^{-1} throughout the outflow jet profile (Fig. 15b). The meridional wind profile in the updraft exhibits a broad poleward maximum of ~ −30 m s^{-1} near 9 km (Fig. 15a), again such that w/v is approximately constant. The meridional wind profile near the outflow jet exhibits weak flow in the middle and lower troposphere and a strong poleward flow in the layer 9–15 km, with a maximum of ~ −34 m s^{-1} near 14 km (Fig. 15b).

Figure 16 shows a sequence of meridional wind profiles following the location of the maximum in horizontal wind speed for the period 0720–1400 UTC 10 April 2014. The first profile exhibits a speed maximum near 6 km, with subsequent profiles showing the momentum surge being transported in the updraft to ~14.5 km, and then subsiding to ~14 km. The maximum meridional velocity increases from −22 to −40 m s^{-1} during this convective momentum surge, or ~1 m s^{-1} every 20 min.

8. Discussion of convective momentum transport hypothesis and PV budget

The cases presented in sections 5–7 support the convective momentum transport hypothesis depicted in Fig. 3b, where midtropospheric cyclonic flow is injected into the base of the stratosphere, yielding a jetlet that opposes the ambient flow (Fig. 4). It is consistent with the momentum surges depicted in Figs. 8, 12, and 16, where acceleration of midtropospheric flow in an updraft leads to acceleration of a jetlet in the UTLS, generating a PV dipole. The orientation of the jetlet is directly related to the direction of motion of the air in the updraft.

The transition from troposphere to stratosphere is similar to that between water and air for a canoe paddle, such that a momentum pulse impinging on the interface will yield a local jetlet, hence a vorticity dipole. This point of view is closely related to human experience. An advantage of this perspective is that one only need know the wind profiles in an updraft and ambient air in order

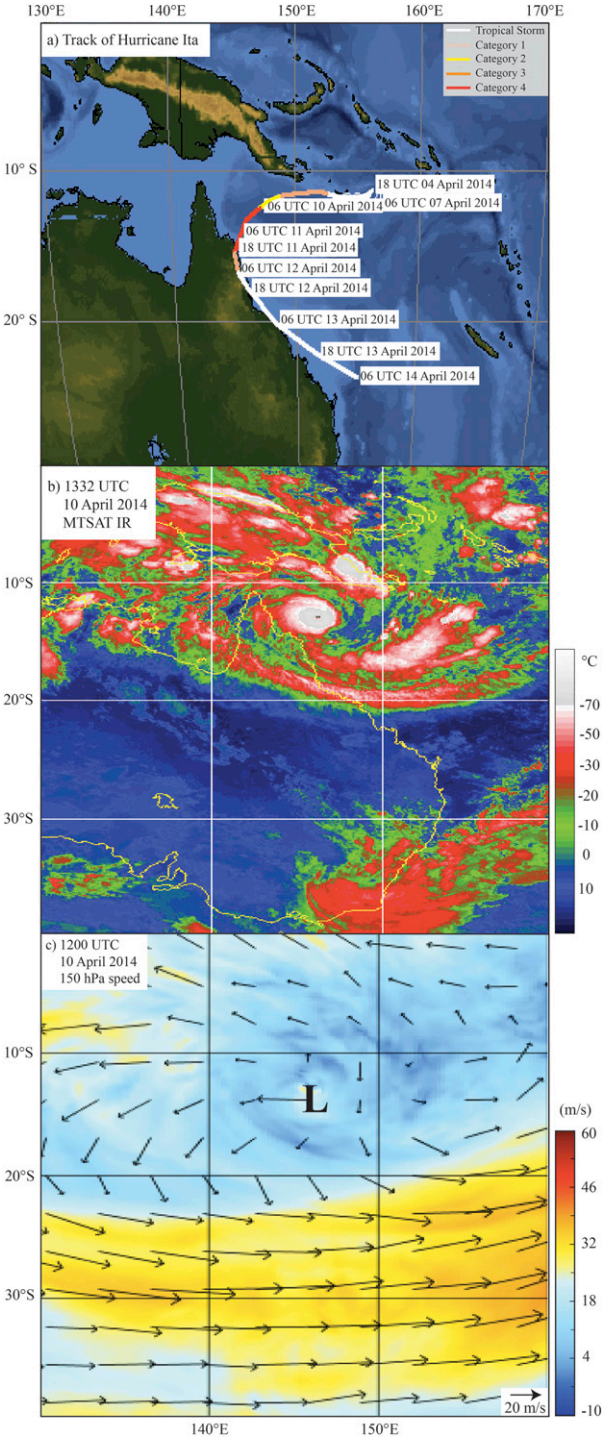

FIG. 13. (a) Track of Hurricane Ita during 4–14 Apr 2014. (b) MTSAT infrared image at 1332 UTC 10 Apr 2014, courtesy of SSEC. (c) ECMWF 150 hPa winds (color bar, reference vector 20 m s^{-1}) at 1200 UTC 10 Apr 2014.

to determine the orientation of a UTLS jetlet/PV dipole. It is closely related to the vorticity tilting hypothesis, but does not require knowledge of the synoptic-scale wind structure and horizontal vorticity field. This perspective takes account of the fact that the UTLS PV dipole does not extend below the base of the outflow jet. It also emphasizes the fact that, in convective asymmetries, horizontal wind speeds accelerate within the updraft relative to surrounding air.

What accounts for the magnitude and vertical extent of UTLS PV dipole/jetlets? One may use Figs. 6, 10, and 14 to estimate the spatial variation across a jetlet: $\delta v/\delta x \sim \pm 30\,\mathrm{m\,s^{-1}}\,(150\,\mathrm{km})^{-1} \sim \pm 2\times10^{-4}\,\mathrm{s^{-1}}$. In the lowest subtropical stratosphere, $(1/\rho)(\partial\theta/\partial z) \sim 0.2\,\mathrm{K\,m^2\,kg^{-1}}$, which is ~20 times larger than in the midtroposphere, using values from Grise et al. (2010). Thus, one would expect PV dipoles $\sim \pm 20$ PVU to exist, as shown. Vertical motion does not penetrate very far into the stratosphere, limiting the upward extent of the PV dipole. The lower limit of the vertical extent of the PV dipole is determined by the lower limit of the outflow jet. The dipole maxima lie slightly above the outflow maximum due to the rapid upward increase in $(1/\rho)(\partial\theta/\partial z)$.

This process can be represented as a source term in the PV conservation equation. A local horizontal jet impinging on the base of the stratosphere will create a spatially varying force due to the gradient in stress [**F** in (2)] in the UTLS. In isentropic coordinates, Ertel's potential vorticity $P = (\zeta + f)/\sigma$ can change following the motion due to a curl of the "viscous force" and terms related to vertical gradients in heating:

$$\frac{dP}{dt} = \frac{1}{\sigma}\left(\frac{\partial F_y}{\partial x} - \frac{\partial F_x}{\partial y}\right) + P\frac{\partial Q}{\partial \theta} + \frac{1}{\sigma}\left(\frac{\partial Q}{\partial y}\frac{\partial u}{\partial \theta} - \frac{\partial Q}{\partial x}\frac{\partial v}{\partial \theta}\right), \tag{4}$$

where $Q = d\theta/dt$ is the schematic view of the process (Andrews et al. 1987, appendix 3A). Consider a force applied to the base of the stratosphere in the shape of a northward jetlet. East of the jetlet, $\partial F_y/\partial x < 0$, which would spin up a negative anomaly, while west of the jetlet, $\partial F_y/\partial x > 0$, which would spin up a positive anomaly, as in Fig. 3b. Magnitudes on the rhs of (4) will be estimated below.

Numerical gridpoint models can provide momentum flux estimates but do not distinguish between updraft and ambient air. To ask the question of how deep convection influences its environment, one must impose a conceptual distinction. Acceleration of "ambient" air from the spatial gradient in stress $\tau = \rho v_u w_u$ due to a tilted updraft may be estimated from

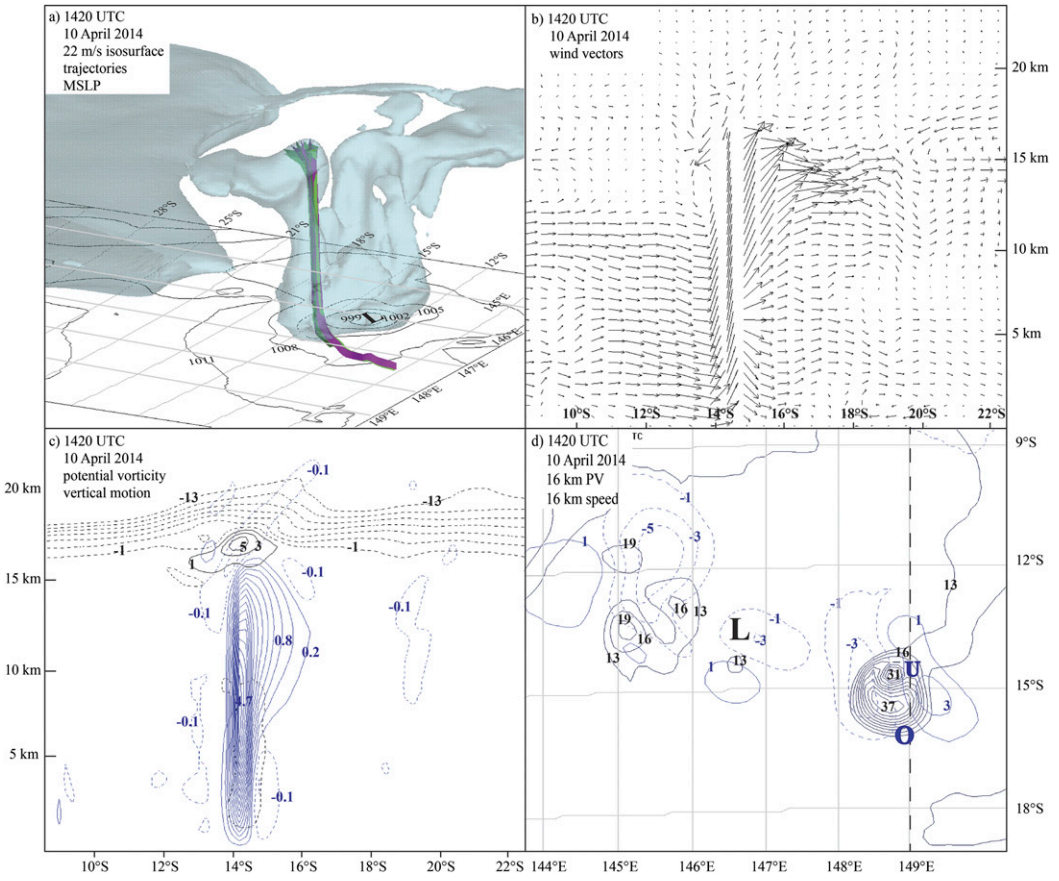

FIG. 14. UWNMS simulation of Hurricane Ita at 1420 UTC 10 Apr 2014. (a) View from the northeast of the 22 m s^{-1} 3D speed isosurface (blue), SLP (contours every 4 hPa), and 2-h back trajectories from the location of the PV dipole (purple ribbons). (b) Meridional section through the updraft in (a) of wind vectors in the plane. (c) Meridional section of vertical motion (blue contours, every 0.3 m s^{-1}) and PV (black contours, every 2 PVU). (d) 16 km wind speed (black contours every 3 m s^{-1}) and PV (blue contours every 1 PVU). The location of the surface low ("L") is shown. South is to the right in panels (b),(c).

$$\frac{\partial v_a}{\partial t} \sim F_y \sim \frac{1}{\rho}\frac{\partial \tau}{\partial z} = -\frac{1}{\rho}\frac{\partial(\rho v_u w_u)}{\partial z}. \qquad (5)$$

Figure 17a shows a meridional section of vw through the tilted updraft in the Edouard PV dipole (Fig. 10), which may be considered to be $v_u w_u$ in the updraft. The poleward tilt of the updraft implies an upward transport of poleward momentum, reaching ~80 m^2 s^{-2} in the upper troposphere. The upward flux of poleward momentum is associated with the wind speed maximum in the updraft (Fig. 17b). Weak downward momentum transport is associated with the subsiding outflow jet (Figs. 17a,b). From (5), an upward decrease of 70 m^2 s^{-2} in 5 km suggests a poleward acceleration of ~1 m s^{-1} per minute in the outflow jet. However, the UWNMS does not distinguish between the updraft and ambient air, so the appropriate interpretation is that the acceleration is due to vertical advection, which for $w \sim 2$ m s^{-1} and $\partial v/\partial z \sim 30$ m s^{-1} per 5000 m gives $\partial v/\partial t \sim -w(\partial v/\partial z) \sim$ 1 m s^{-1} per minute. This is sufficient to account for observed acceleration in the outflow jet.

The first term on the rhs of (4) may be estimated based on a poleward acceleration of $F_y \sim 1$ m s^{-1} per minute, a perpendicular spatial scale for the jet of ~100 km, and $\sigma^{-1} \sim 5$ kg K^{-1} m^{-2} in the UTLS: $dP/dt \sim 1$ PVU per minute, which is sufficient to achieve formation of a PV dipoles of the observed magnitude in less an hour. Considering the term $P(\partial Q/\partial\theta)$ in (4), in the UTLS, Q is generally less than a few kelvin per day (Andrews et al. 1987). If the variation in Q is as strong as ~1 K day^{-1} across 10 K, with $P \sim 10$ PVU, this term is only ~1 PVU per day. This is similar to magnitudes found by Chagnon et al. (2013) for radiative heating patterns near cloud tops in MCs. Similarly, an estimate of the third term in (4), taking the vertical scale of velocity variation to be 1 m s^{-1} per km, yields ~1 PVU per day. This suggests that the spatially varying tangential force associated with the stress gradient, caused

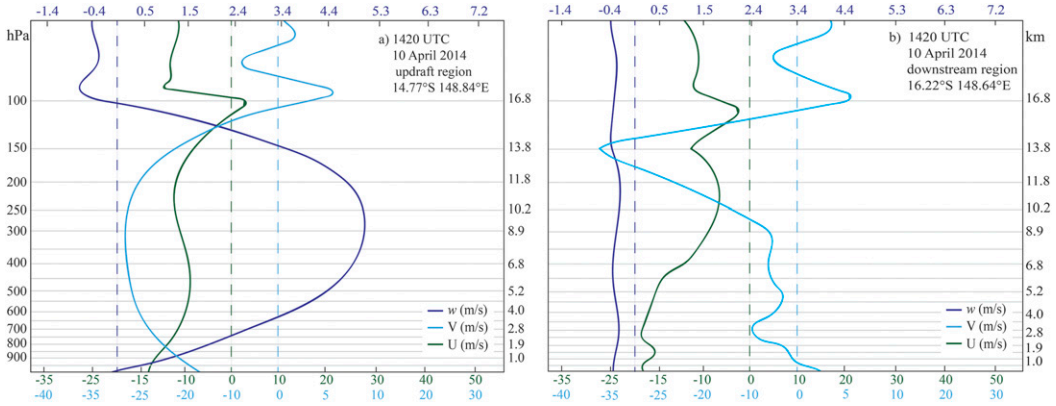

FIG. 15. As in Fig. 7, but for the Ita PV dipole/jetlet shown in Fig. 14, at 1420 UTC 10 Apr 2014.

by an impinging jetlet in (4), is many orders of magnitude larger than the terms involving diabatic heating, and that it is the most likely physical mechanism that can create a UTLS PV dipole in an hour or so.

9. TC energetics and asymmetric distribution of winds

a. *Thermodynamic acceleration*

Density anomalies, ρ', determine buoyancy and vertical acceleration, as represented by the Boussinesq approximation to 2c: $dw/dt = -g - (1/\rho)(\partial p/\partial z) \approx -(\rho'/\overline{\rho})\,g$. Moisture and latent heat release exert a strong control over ρ'. The rate of change of vertically integrated density is equal to the rate of change in SLP. Divergence aloft accompanies a fall in central SLP, which accelerates radial inflow and further ingestion of warm, moist air. This synergistic feedback between latent heat release, vertical and horizontal acceleration may be termed ''thermodynamic acceleration.'' This can occur in axisymmetric TCs or in a local convective complex.

A meridional section (along the dashed line in Fig. 10d) of perturbation density, ρ', where the domain average profile, $\overline{\rho}$, has been subtracted, is shown for the Edouard case in Fig. 17b. In the lower troposphere, ρ' decreases toward the updraft and upward to the midtroposphere within the updraft, consistent with inward and upward acceleration, maximizing near the level of maximum latent heating. Above the midtroposphere, the density anomaly and vertical acceleration become smaller. A sharp maximum in density anomaly is seen at the top of the overshooting updraft, consistent with deceleration. The outflow jet then subsides quasi-isentropically along the base of the positive density anomaly.

Note the cross-isobaric flow evident in the trajectories in Figs. 6a, 10a, and 14a, as they accelerate into the updrafts. Since latent heat release is concentrated in the convective complex, inward and upward acceleration will be stronger, so that the air in the updraft will have higher horizontal speed than the surrounding air. The cyclonic momentum in the convective complex will then be transported and mixed throughout the storm, perhaps tending to strengthen the TC as a whole.

b. *Azimuthal asymmetries in winds*

Poleward surges and jetlet formation are intimately linked with the dynamics of convective asymmetries. Examples of mesoscale wind variations and storm-scale azimuthal asymmetries are shown in Fig. 18. Difference profiles between the meridional wind component in the updraft and in the outflow jet, $v_u(z) - v_o(z)$, are shown for each case, along with maps of PV and winds at 7 km. Significant azimuthal asymmetries in cyclonic winds are

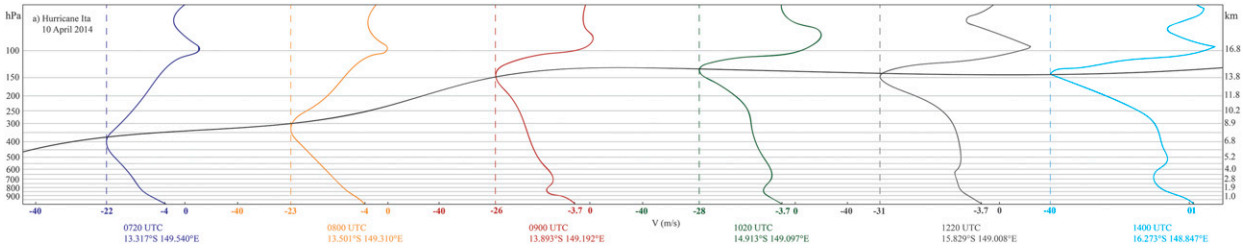

FIG. 16. As in Fig. 8, but for the Ita PV dipole/jetlet shown in Fig. 14, for the period 0720–1400 UTC 10 Apr 2014.

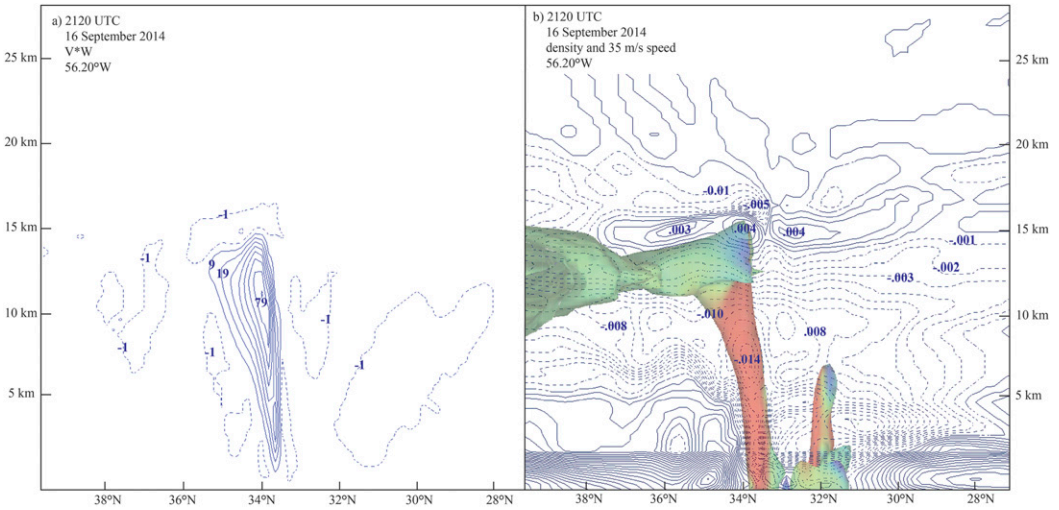

FIG. 17. Latitude–altitude section through the dipole in Hurricane Edouard (Fig. 10) at 2120 UTC 16 Sep 2014 of (a) vw (contour interval $10\,m^2\,s^{-2}$ starting at -1) and (b) density anomaly (contour interval $0.001\,kg\,m^{-3}$) and a $30\,m\,s^{-1}$ speed isosurface colored by the value of vw (red/yellow positive, blue/green negative).

apparent (Figs. 18b,d,f). The poleward surge associated with each updraft near 7 km (Figs. 18b,d,f) is consistent with the profiles (Figs. 18a,c,e), where midtropospheric poleward flow in the updraft is $\sim 20\,m\,s^{-1}$ faster than in the outflow region.

The speed range in the profile differences across $\sim$100 km is $\sim$20–50 $m\,s^{-1}$ at most altitudes (Figs. 18a,c,e), suggesting typical magnitudes of vorticity and shear of $\sim 2\text{–}5 \times 10^{-4}\,s^{-1}$. The speed in the outflow jet exceeds that of the air in the updraft at the same level by $\sim 50\,m\,s^{-1}$ in Talas (Fig. 18a), $\sim 20\,m\,s^{-1}$ in Edouard (Fig. 18c), and $\sim 15\,m\,s^{-1}$ in Ita (Fig. 18e). Both the outflow jet and the updraft are moving faster than their environment.

The effect that local acceleration in convective complexes has on the distribution of radial and tangential winds may be seen in N–S and E–W sections through the centers of Talas, Edouard, and Ita (Fig. S4). Meridional sections of UWNMS meridional wind through the center of the TCs show the radial or secondary flow, while zonal sections of meridional wind show the tangential or primary flow. In agreement with axisymmetric models of inflow, radial winds show convergence in the lowest $\sim$2 km, beginning several hundred km from the eye (Figs. S4a,c,e). Noticeable asymmetries in inflow strength and extent may be seen. In the UTLS an outflow layer $\sim$5 km thick extends poleward more than 1000 km.

A maximum in cyclonic flow is found near the top of the inflow layer, in agreement with axisymmetric models. However, winds vary considerably throughout the rest of each TC and surrounding troposphere. These results are in general agreement with recent work cited in section 2. Flow in convective complexes with large accelerations will have Ro ≥ 1, so one would not expect the flow to be in thermal wind balance. Local accelerations are thermally direct, and cannot be determined by considerations of thermal wind balance.

10. Conclusions

Diagnosis of three case studies of UTLS PV dipole/jetlets reveals that their formation is intimately related to horizontal wind speed maxima, which are transported upward in updrafts, and ejected into the UTLS. A spatially continuous speed maximum is observed to travel from upstream in the lower troposphere, accelerating in the tilted updraft, and into the outflow jet. Wind profiles and speed isosurfaces show that both vertical and azimuthal velocity maximize in the midtroposphere in the updraft, ensuring a fairly uniform tilt with height. Cyclonic momentum in the midtroposphere is transported upward in the updraft and becomes a mesoscale outflow jet directed in the same sense.

The cases support our hypothesis of convective momentum transport, as UTLS jetlets are observed to be cyclonic in TCs, thus implying that anticyclonic PV will lie to the right, or radially outward. The spatial confinement of the horizontal speed maximum in the updraft is consistent with the idea that a vorticity dipole will be created when the jetlet reaches the base of the stratosphere, induced by the curl of the force arising from the stress gradient exerted by the jetlet. The sharp vertical confinement of the PV dipole and jetlet to the UTLS is explained by the strong static stability of the stratosphere, confining it to a $\sim$5 km deep outflow layer

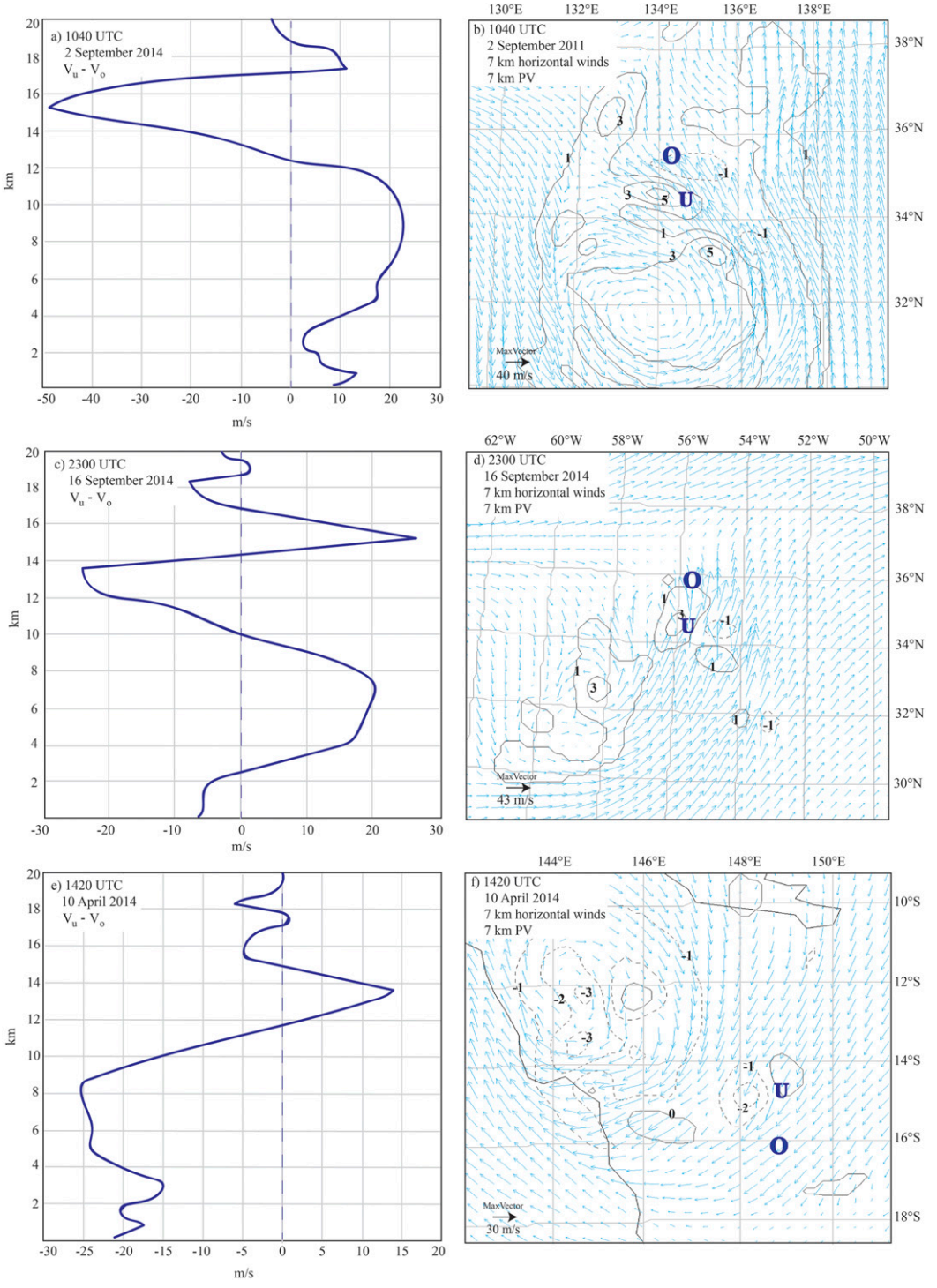

FIG. 18. (left) UWNMS difference profiles between meridional wind in the updraft (“U”) and 150 km downstream in the outflow jet (“O”), $v_u(z) - v_o(z)$, for the case of (a) Talas at 1040 UTC 2 Sep 2011 (Fig. 6d), (c) Edouard at 2300 UTC 16 Sep 2014 (Fig. 10d), and (e) Ita at 1420 UTC 10 Apr 2014 (Fig. 14d). In the troposphere, the poleward flow in the updraft exceeds that in the environment. In the UTLS, the speed in the outflow jet downstream exceeds that of the air near the top of the updraft. (right) UWNMS 7 km PV (black contours) and horizontal wind vectors for each case. The contour interval is 1 PVU in (b) and 2 PVU in (d),(f). The maximum wind vector is 30 m s^{-1} in (b), 40 m s^{-1} in (d), and 43 m s^{-1} in (f).

in the UTLS. The outflow jet maximizes just below the altitude of maximum PV dipole strength and below the positive density anomaly. Estimates of momentum flux convergence and of vertical advection near the top of the tilted updraft are consistent with poleward acceleration observed in the outflow jet. Estimates of PV forcing by the curl of the ''net viscous force'' supports the idea that this mechanism can account for creation of the observed PV dipoles.

The idea of local thermodynamic acceleration is used to explain the observed horizontal acceleration within an updraft, such that local maxima in wind speed are injected into the UTLS and mixed into the broader environment. Convective asymmetries are characterized by strong mesoscale and azimuthal variation in radial and tangential winds. A summary of the processes involved in the formation of UTLS jetlet/PV dipoles includes: First, a local momentum surge occurs in the lower troposphere associated with inflow into a region of enhanced deep convection, fueled by latent heat release. Second, the horizontal speed maximum undergoes further acceleration as it is carried upward in the poleward-tilting updraft, and is injected into the UTLS. Third, the horizontally moving updraft impinging on the stratosphere creates a mesoscale jet and associated horizontal PV dipole. Finally, the speed maximum extends radially outward from the jetlet, sometimes joining with the SWJ. It is of interest to further investigate the role of PV dipole/jetlets and convective asymmetries in the evolution of TCs.

Acknowledgments. We are grateful for support from NSF Grant AGS-1555851. ECMWF data were acquired from NCAR, which is funded by NSF. Satellite images are courtesy of SSEC, University of Wisconsin–Madison. We also thank Tim Dunkerton and two anonymous reviewers for their helpful comments.

REFERENCES

Abarca, S. F., M. T. Montgomery, S. A. Braun, and J. Dunion, 2016: On the secondary eyewall formation of Hurricane Edouard (2014). *Mon. Wea. Rev.*, **144**, 3321–3331, https://doi.org/10.1175/MWR-D-15-0421.1.

Andrews, D. G., J. R. Holton, and C. B. Leovy, 1987: *Middle Atmosphere Dynamics*. Academic Press, 489 pp.

Austin, P. M., and R. A. Houze Jr., 1973: A technique for computing vertical transports by precipitating cumuli. *J. Atmos. Sci.*, **30**, 1100–1111, https://doi.org/10.1175/1520-0469(1973)030<1100:ATFCVT>2.0.CO;2.

Bosart, L. F., W. E. Bracken, J. Molinari, C. S. Velden, and P. G. Black, 2000: Environmental influences on the rapid intensification of Hurricane Opal (1995) over the Gulf of Mexico. *Mon. Wea. Rev.*, **128**, 322–352, https://doi.org/10.1175/1520-0493(2000)128<0322:EIOTRI>2.0.CO;2.

Carrier, G. F., 1971: The intensification of hurricanes. *J. Fluid Mech.*, **49**, 145–158, https://doi.org/10.1017/S0022112071001976.

Chagnon, J. M., and S. L. Gray, 2009: Horizontal potential vorticity dipoles on the convective storm scale. *Quart. J. Roy. Meteor. Soc.*, **135**, 1392–1408, https://doi.org/10.1002/qj.468.

——, ——, and J. Methven, 2013: Diabatic processes modifying potential vorticity in a North Atlantic cyclone. *Quart. J. Roy. Meteor. Soc.*, **139**, 1270–1282, https://doi.org/10.1002/qj.2037.

Charney, J. G., and A. Eliassen, 1964: On the growth of the hurricane depression. *J. Atmos. Sci.*, **21**, 68–75, https://doi.org/10.1175/1520-0469(1964)021<0068:OTGOTH>2.0.CO;2.

CIMSS, 2018: Index of /real-time/satcon/archive. Cooperative Institute for Meteorological Satellite Studies, accessed 27 June 2018, tropic.ssec.wisc.edu/real-time/satcon/archive.

Davies-Jones, R., 1984: Streamwise vorticity: The origin of updraft rotation in supercell storms. *J. Atmos. Sci.*, **41**, 2991–3006, https://doi.org/10.1175/1520-0469(1984)041<2991:SVTOOU>2.0.CO;2.

Didlake, A. C., and R. A. Houze Jr., 2011: Kinematics of the secondary eyewall observed in Hurricane Rita (2005). *J. Atmos. Sci.*, **68**, 1620–1636, https://doi.org/10.1175/2011JAS3715.1.

——, G. M. Heymsfield, P. D. Reasor, and S. R. Guimond, 2017: Concentric eyewall asymmetries in Hurricane Gonzalo (2014) observed by airborne radar. *Mon. Wea. Rev.*, **145**, 729–749, https://doi.org/10.1175/MWR-D-16-0175.1.

——, P. D. Reasor, R. F. Rogers, and W.-C. Lee, 2018: Dynamics of the transition from spiral rainbands to a secondary eyewall in Hurricane Earl (2010). *J. Atmos. Sci.*, **75**, 2909–2929, https://doi.org/10.1175/JAS-D-17-0348.1.

Emanuel, K. A., 1986: An air-sea interaction theory for tropical cyclones. Part I: Steady-state maintenance. *J. Atmos. Sci.*, **43**, 585–605, https://doi.org/10.1175/1520-0469(1986)043<0585:AASITF>2.0.CO;2.

Fang, J., and F. Zhang, 2011: Evolution of multiscale vortices in the development of Hurricane Dolly (2008). *J. Atmos. Sci.*, **68**, 103–122, https://doi.org/10.1175/2010JAS3522.1.

——, O. Pauluis, and F. Zhang, 2017: Isentropic analysis on the intensification of Hurricane Edouard (2014). *J. Atmos. Sci.*, **74**, 4177–4197, https://doi.org/10.1175/JAS-D-17-0092.1.

Frisius, T., 2015: What controls the size of a tropical cyclone? Investigations with an axisymmetric model. *Quart. J. Roy. Meteor. Soc.*, **141**, 2457–2470, https://doi.org/10.1002/qj.2537.

Grise, K. M., D. W. J. Thompson, and T. Birner, 2010: A global survey of static stability in the stratosphere and upper troposphere. *J. Climate*, **23**, 2275–2292, https://doi.org/10.1175/2009JCLI3369.1.

Guimond, S. R., G. M. Heymsfield, and F. J. Turk, 2010: Multiscale observations of Hurricane Dennis (2005): The effects of hot towers on rapid intensification. *J. Atmos. Sci.*, **67**, 633–654, https://doi.org/10.1175/2009JAS3119.1.

Hernandez-Duenas, G., L. M. Smith, and S. N. Stechmann, 2014: Investigation of Boussinesq dynamics using intermediate models based on wave–vertical interactions. *J. Fluid Mech.*, **747**, 247–287, https://doi.org/10.1017/jfm.2014.138.

Heymsfield, G. M., J. B. Halverson, J. Simpson, L. Tian, and T. P. Bui, 2001: ER-2 Doppler radar investigations of the eyewall of Hurricane Bonnie during the Convection and Moisture Experiment-3. *J. Appl. Meteor.*, **40**, 1310–1330, https://doi.org/10.1175/1520-0450(2001)040<1310:EDRIOT>2.0.CO;2.

Hitchman, M. H., M. L. Buker, and G. J. Tripoli, 1999: Influence of synoptic waves on column ozone during Artic summer 1997. *J. Geophys. Res.*, **104**, 26 547–26 563, https://doi.org/10.1029/1999JD900471.

——, ——, ——, R. B. Pierce, J. A. Al-Saadi, E. V. Bromwell, and M. A. Avery, 2004: A modeling study of an East Asian convective complex during March 2001. *J. Geophys. Res.*, **109**, D15S14, https://doi.org/10.1029/2003JD004312.

——, and S. M. Rowe, 2017: On the similarity of lower stratospheric potential vorticity dipoles above tropical and midlatitude deep convection. *J. Atmos. Sci.*, **74**, 2593–2613, https://doi.org/10.1175/JAS-D-16-0239.1.

——, M. L. Buker, G. J. Tripoli, E. V. Browell, W. B. Grant, T. J. McGee, and J. F. Burris, 2003: Nonorographic generation of Arctic polar stratospheric clouds during December 1999. *J. Geophys. Res.*, **108**, 8325, https://doi.org/10.1029/2001JD001034.

Holland, G. J., and R. T. Merrill, 1984: On the dynamics of tropical cyclone structural changes. *Quart. J. Roy. Meteor. Soc.*, **110**, 723–745, https://doi.org/10.1002/qj.49711046510.

Houze, R. A., Jr., W. C. Lee, and M. M. Bell, 2009: Convective contribution to the genesis of Hurricane Ophelia (2005). *Mon. Wea. Rev.*, **137**, 2778–2800, https://doi.org/10.1175/2009MWR2727.1.

Huang, Y.-H., C.-C. Wu, and M. T. Montgomery, 2018: Concentric eyewall formation in Typhooon Sinlaku (2008). Part III: Horizontal momentum budget analyses. *J. Atmos. Sci.*, **75**, 3541–3563, https://doi.org/10.1175/JAS-D-18-0037.1.

Japan Meteorological Agency, 2011: Annual report on the activities of the RSMC Tokyo–Typoon Center 2011. Japan Meteorological Agency, 82 pp., http://www.jma.go.jp/jma/jma-eng/jma-center/rsmc-hp-pub-eg/AnnualReport/2011/Text/Text2011.pdf.

Kittaka, C., and Coauthors, 2004: A three-dimensional regional modeling study of the impact of clouds on sulfate distributions during TRACE-P. *J. Geophys. Res.*, **109**, D15S11, https://doi.org/10.1029/2003JD004353.

Komaromi, W. A., and J. D. Doyle, 2017: Tropical cyclone outflow and warm core structure as revealed by HS3 dropsonde data. *Mon. Wea. Rev.*, **145**, 1339–1359, https://doi.org/10.1175/MWR-D-16-0172.1.

Malkus, J. S., 1952: The slopes of cumulus clouds in relation to external wind shear. *Quart. J. Roy. Meteor. Soc.*, **78**, 530–542, https://doi.org/10.1002/qj.49707833804.

Markowski, P., and Y. Richardson, 2010: *Mesoscale Meteorology in Midlatitudes*. John Wiley and Sons, 407 pp.

Molinari, J., and D. Vollaro, 2010: Distribution of helicity, CAPE, and shear in tropical cyclones. *J. Atmos. Sci.*, **67**, 274–284, https://doi.org/10.1175/2009JAS3090.1.

Montgomery, M. T., and R. K. Smith, 2014: Paradigms for tropical cyclone intensification. *Aust. Meteor. Ocean J.*, **64**, 37–66, https://doi.org/10.22499/2.6401.005.

——, M. E. Nicholls, T. A. Cram, and A. B. Saunders, 2006: A vortical hot tower route to tropical cyclogenesis. *J. Atmos. Sci.*, **63**, 355–386, https://doi.org/10.1175/JAS3604.1.

Oku, Y., J. Yoshino, T. Takemi, and H. Ishikawa, 2014: Assessment of heavy rainfall-induced disaster potential based on an ensemble simulation of Typhoon Talas (2011) with controlled track and intensity. *Nat. Hazards Earth Syst. Sci.*, **14**, 2699–2709, https://doi.org/10.5194/nhess-14-2699-2014.

Ooyama, K., 1964: A dynamical model for the study of tropical cyclone development. *Geofis. Int.*, **4**, 187–198.

——, 1969: Numerical simulation of the life cycle of tropical cyclones. *J. Atmos. Sci.*, **26**, 3–40, https://doi.org/10.1175/1520-0469(1969)026<0003:NSOTLC>2.0.CO;2.

Persing, J., M. T. Montgomery, J. C. McWilliams, and R. K. Smith, 2013: Asymmetric and axisymmetric dynamics of tropical cyclones. *Atmos. Chem. Phys.*, **13**, 12 299–12 341, https://doi.org/10.5194/acp-13-12299-2013.

Pokrandt, P. J., G. J. Tripoli, and D. D. Houghton, 1996: Processes leading to the formation of mesoscale waves in the Midwest cyclone of 15 December 1987. *Mon. Wea. Rev.*, **124**, 2726–2752, https://doi.org/10.1175/1520-0493(1996)124<2726:PLTTFO>2.0.CO;2.

Rappin, E., M. C. Morgan, and G. J. Tripoli, 2011: The impact of outflow environment on tropical cyclone intensification and structure. *J. Atmos. Sci.*, **68**, 177–194, https://doi.org/10.1175/2009JAS2970.1.

Reasor, P. D., R. Rogers, and S. Lorsolo, 2013: Environmental flow impacts on tropical cyclone structure diagnosed from airborne Doppler radar composites. *Mon. Wea. Rev.*, **141**, 2949–2969, https://doi.org/10.1175/MWR-D-12-00334.1.

Rogers, R. F., J. A. Zhang, J. Zawislak, H. Jiang, G. R. Alvey, E. J. Zipser, and S. N. Stevenson, 2016: Observations of the structure and evolution of Hurricane Edouard (2014) during intensity change. Part II: Kinematic structure and the distribution of deep convection. *Mon. Wea. Rev.*, **144**, 3355–3376, https://doi.org/10.1175/MWR-D-16-0017.1.

Rowe, S. M., and M. H. Hitchman, 2015: On the role of inertial instability in stratosphere–troposphere exchange in midlatitude cyclones. *J. Atmos. Sci.*, **72**, 2131–2151, https://doi.org/10.1175/JAS-D-14-0210.1.

——, and ——, 2016: On the relationship between inertial instability, poleward momentum surges, and jet intensifications near midlatitude cyclones. *J. Atmos. Sci.*, **73**, 2299–2315, https://doi.org/10.1175/JAS-D-15-0183.1.

Smith, R. K., M. T. Montgomery, and J. Persing, 2014: On steady-state tropical cyclones. *Quart. J. Roy. Meteor. Soc.*, **140**, 2638–2649, https://doi.org/10.1002/qj.2329.

Snyder, C. D., D. J. Muraki, R. Plougonven, and F. Zhang, 2007: Inertia–gravity waves generated within a dipole vortex. *J. Atmos. Sci.*, **64**, 4417–4431, https://doi.org/10.1175/2007JAS2351.1.

Van Sang, N., R. K. Smith, and M. T. Montgomery, 2008: Tropical-cyclone intensification and predictability in three dimensions. *Quart. J. Roy. Meteor. Soc.*, **134**, 563–582, https://doi.org/10.1002/qj.235.

Wang, Z., 2014: Characteristics of convective processes and vertical vorticity from the tropical wave to tropical cyclone stage in a high-resolution numerical model simulation of Tropical Cyclone Fay (2008). *J. Atmos. Sci.*, **71**, 896–915, https://doi.org/10.1175/JAS-D-13-0256.1.

Willoughby, H. E., 1995: Mature structure and evolution. *Global Perspectives on Tropical Cyclones*, R. L. Elsberry, Ed., World Meteorological Organization, 21–62.

Wirth, V., and T. J. Dunkerton, 2006: A unified perspective on the dynamics of axisymmetric hurricanes and monsoons. *J. Atmos. Sci.*, **63**, 2529–2547, https://doi.org/10.1175/JAS3763.1.

Wu, C.-C., and H.-J. Cheng, 1999: An observational study of environmental influences on the intensity changes of Typhoons Flo (1990) and Gene (1990). *Mon. Wea. Rev.*, **127**, 3003–3031, https://doi.org/10.1175/1520-0493(1999)127<3003:AOSOEI>2.0.CO;2.